Numerical Investigation of Transients in the SSPX Spheromak

C. R. Sovinec,[1] B. I. Cohen,[2] G. A. Cone,[1] E. B. Hooper,[2] and H. S. McLean[2]
[1]University of Wisconsin, Madison, Wisconsin 53706, USA
[2]Lawrence Livermore National Laboratory, Livermore, California 94550, USA
(Received 13 October 2004; published 24 January 2005)

Nonlinear plasma simulations of the Sustained Spheromak Physics Experiment demonstrate the role of transient effects in establishing a toroidal magnetic structure that confines internal energy. Magnetohydrodynamics modeling with temperature-dependent transport coefficients compares well with experimental measurements and shows that the second current pulse improves confinement by keeping the q profile from falling below the value of $1/2$, suppressing resonant $m = 1$, $n = 2$ fluctuations.

DOI: 10.1103/PhysRevLett.94.035003 PACS numbers: 52.55.Ip, 52.35.Py, 52.65.Kj

Magnetic reconnection and relaxation are elemental processes for electrostatically driven spheromaks. The plasma conducts electrical current between electrodes linked by open magnetic field lines, and nonlinear effects convert toroidal magnetic flux into poloidal flux [1–3]. While inductive effects can contribute to formation, symmetry-breaking magnetic fluctuations are required for sustainment [4,5], as found experimentally in SPHEX [6]. The flux conversion process is reproduced by nonlinear resistive magnetohydrodynamics (MHD) computations [7], and the numerical results show chaotic scattering of open magnetic field lines throughout the plasma when the spheromak is sustained [8]. The computations also demonstrate a topological change to closed magnetic-flux surfaces during decay [7], consistent with measurements such as the record of 400 eV [9] obtained subsequent to the electrostatic injection pulse. However, temperatures exceeding 100 eV are also observed in the Sustained Spheromak Physics Experiment (SSPX) [10] during application of a second current pulse [11,12], though temperatures resulting from Ohmic heating with classical parallel transport are limited to tens of eV [13–15] in open-field configurations.

Here we investigate the role of transient effects in SSPX energy confinement. We consider a single-fluid model with temperature-dependent thermal conduction and electrical resistivity in the SSPX vacuum chamber geometry and apply a simulated injector-current waveform that approximates discharges Nos. 4620–4662 [11]. The temperature and magnetic fields are tightly coupled; magnetic topology and parallel thermal conduction regulate energy confinement, while resistivity influences magnetic reconnection and diffusion. The length of open magnetic field lines and the extent of any region of closed magnetic flux are governed dynamically by MHD instabilities, which respond quickly to changes in the parallel current density distribution.

The simulations of SSPX solve nonlinear time-dependent equations for particle number density ($n_i = n_e = n$ with quasineutrality), plasma flow velocity, temperature (assuming $T_i = T_e = T$), and magnetic field ($\mathbf{B}$); see Ref. [16]. The parallel and perpendicular thermal diffusivities are $\chi_{\parallel} = 387T^{5/2}\ \mathrm{m^2/s}$ and $\chi_{\perp} = 0.50\langle T\rangle^{-1/2}\langle B\rangle^{-2}\ \mathrm{m^2/s}$ (B in Tesla) based on electrons and ions [17], respectively, for a hydrogen plasma at $n = 5 \times 10^{19}\ \mathrm{m^{-3}}$. (The toroidal average, indicated by $\langle\ \rangle$, is used to simplify less sensitive computations.) The electrical diffusivity is computed as $\eta/\mu_0 = 411(1\,\mathrm{eV}/\langle T\rangle)^{3/2}\ \mathrm{m^2/s}$. An isotropic viscosity of $2000\ \mathrm{m^2/s}$ is used to provide nonlinear numerical stability during the full-power stage of the evolution when the Lundquist number ($\mu_0 R \nu_A/\eta$, where $R = 0.5$ m and ν_A is the Alfvén speed) reaches 10^6. A diffusion term in the continuity equation [16] substitutes for particle transport and atomic fueling effects, and the artificial particle diffusivity of $2000\ \mathrm{m^2/s}$ helps keep the computed minimum of n above zero during the violent full-power stage.

The conductive heat-flux model in our MHD simulations applies to collisional plasmas [17] with rapid electron-ion thermal equilibration; parallel (perpendicular) conduction is computed from the relation for electrons (ions). Near the electrodes, the temperature is on the order of 1 eV or less, so the edge plasma is very collisional, and parallel conduction to the edge tends to cool interior plasma. The effective collisional mean free path is $4 \times 10^{-4}T^2$ m (T in eV) [17] for $n \cong 5 \times 10^{19}\ \mathrm{m^{-3}}$ and singly charged ions—less than the radius of SSPX for $T < 35$ eV. Larger temperatures, and hence less collisional conditions, occur only where the open-field lines are very long [13,14] or where closed-flux surfaces form. Since our primary interest is the dynamics that lead to improving energy confinement, the collisional behavior is most important. However, our model tends to overpredict parallel heat flux [18,19] where high temperatures are achieved, and neglecting neoclassical and turbulence effects causes underestimation of ion perpendicular heat transport in closed-field regions.

The system of nonlinear equations is solved with the NIMROD code, which uses a high-order spatial representation to resolve anisotropies [16]. Our computational domain models the SSPX flux conserver and the downstream end of its plasma gun with 1152 bicubic finite elements.

For the toroidal direction, our finite Fourier series representation includes the $0 \leq n \leq 2$ components for the brief formation period and $0 \leq n \leq 5$ components for the current-decay phase after the formation pulse and during the second current pulse. For convenience, we model the upstream boundary of the gun as an artificial solid wall. The tangential component of electric field is zero on the electrode surfaces, and a time-dependent boundary condition on the toroidal component of $\langle \mathbf{B} \rangle$ along the artificial boundary injects a specified current in the computations [Fig. 1(a)], except during the decay phase, which is simulated as a temporary short circuit. Radiation amounts to a small fraction of the power loss in SSPX [11] and is not modeled, but a sink of internal energy is imposed in computational cells adjacent to the artificial upstream boundary to control the thickness of the resistive boundary layer.

The parallel current density profile is stable to toroidally asymmetric perturbations when mass and poloidal flux are swept out of the gun. While the profile is still stable but becoming pinched at $t = 0.08$ ms, velocity perturbations amounting to 2 J of kinetic energy are introduced in the $n = 1$ and 2 Fourier components of the simulations. At $t \cong 0.09$ ms, the current profile becomes unstable to an $n = 1$ MHD mode, and magnetic fluctuations subsequently grow at a rate of 5×10^5 s^{-1}, which is fast relative to the injector-current transient. Abrupt changes in toroidal plasma current and magnetic energy, evident at $t = 0.1$ ms in Figs. 1(c) and 1(d), occur when the $n = 1$ mode saturates and toroidal flux is converted into poloidal flux [1,7,20]. Flux conversion increases the poloidal flux by 200%, and the injector voltage is very large (> 1 kV) in both the simulation and the experiment during this formation phase [see Fig. 1(b)]. Voltage during the second current-drive pulse is much smaller, 20 V in the simulation and fluctuating around 200 V in the experiment, including the sheath potential of 100–150 V [14,21]. The power during the second current pulse is a small fraction of formation power, but the rates of decay of toroidal current and magnetic energy are reduced [Figs. 1(c) and 1(d)] relative to the period between the two injector-current pulses. Magnetohydrodynamic equilibria fitted to various laboratory measurements after $t = 0.3$ ms using the CORSICA code [10] are in agreement to within 25% for the toroidal current, the magnetic energy, and their rates of decay, as shown in Figs. 1(c) and 1(d).

Magnetic fluctuations are largest during formation, when the $n = 1$ mode relaxes the configuration, and decay rapidly during the subsequent ramp-down. They evolve to their lowest levels [$< 1\%$ at the outer wall; see Fig. 2(a)] during the second current pulse. The $n = 2$ mode is particularly responsive, as shown in Fig. 2(b), which compares magnetic fluctuation energy in simulations with and without a second current pulse. When the second pulse is applied, the energy in the $n = 2$ component decays until $t > 0.8$ ms. Without a second pulse, the $n = 2$ and 4 Fourier components grow to large levels from $t = 0.6$ ms onward. The ''quiescent'' period brought about by the second current pulse correlates with increasing temperatures, as in the experiment [11]. Figure 3(a) compares

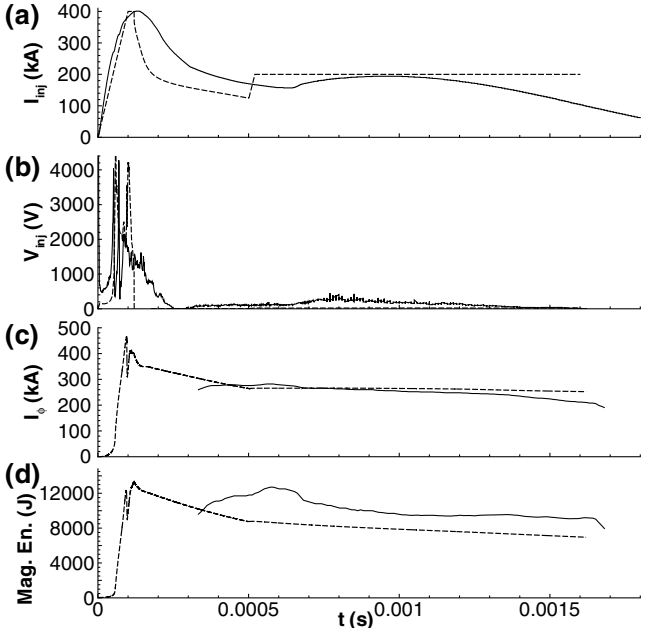

FIG. 1. Evolution of (a) injector current, (b) injector voltage, (c) toroidal current, and (d) stored magnetic energy from SSPX discharge No. 4624 (solid traces) and the simulation (dashed traces). The SSPX results in (c) and (d) are based on a sequence of fitted MHD equilibria.

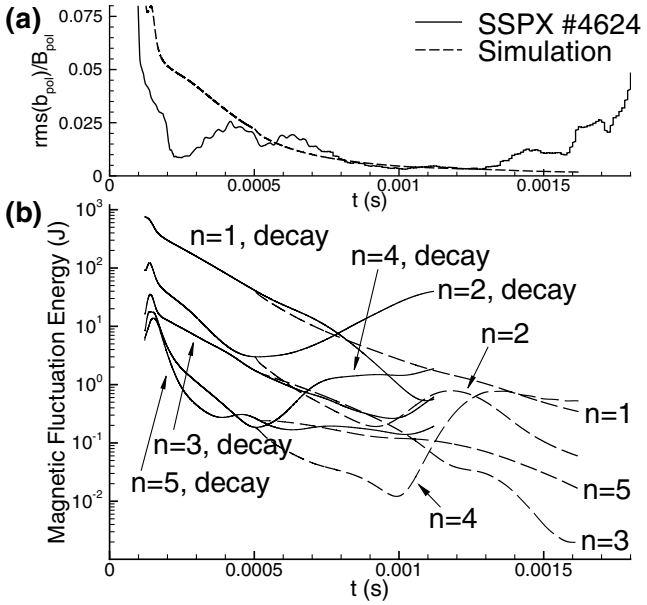

FIG. 2. Magnetic fluctuation information of (a) rms poloidal magnetic fluctuations relative to the equilibrium poloidal field at the outboard midplane probe location from experiment and simulations, and (b) simulated volume-integrated energy by Fourier component. The energy plot shows results with (dashed lines) and without (solid lines) the second current pulse.

Thomson-scattering measurements of central T_e with the evolution of maximum $\langle T \rangle$ from the simulations. While the experiment produced a sharper positive response at $t =$ 1 ms, reaching a maximum of 120 vs 75 eV in the simulation, temperatures also rise substantially with the decline of magnetic fluctuations in the simulation. Without the second current pulse, the single-fluid model produces a maximum temperature of only 49 eV. The profiles in Fig. 3(b) show that energy confinement occurs in a toroidal region, which surrounds relatively cold plasma along the geometric axis.

The discharge appears to be in a sustained state during the second injector pulse [Figs. 1(c) and 1(d)]; however, indefinite sustainment of $\langle J_\phi \rangle$ against resistive dissipation in the region of amplified poloidal flux requires dynamo activity [4]. Dynamo activity in simulations has been demonstrated with a simpler MHD model [7], but it is accompanied by large $n = 1$ fluctuations and chaotic scattering of magnetic field. The present simulations exhibit similar behavior only during the brief formation pulse; near the axis of the amplified poloidal flux, $R \cong 0.35$ m, the toroidal component of fluctuation-induced electric field, $-\langle \mathbf{v} \times \mathbf{b} \rangle$, exceeds $\eta \langle J_\phi \rangle$ by a factor of 50 at $t = 0.12$ ms. During the second injector-current pulse ($t = 1.2$ ms), $-\langle \mathbf{v} \times \mathbf{b} \rangle$ is reduced by more than 3 orders of magnitude, while $\eta \langle J_\phi \rangle$ is only 4 times smaller. Thus, the dynamo activity is far less than what is required for sustainment.

Through anisotropic thermal energy transport, the temperature evolution is a sensitive gauge of the magnetic topology. In Fig. 4, we compare T profiles and Poincaré plots of $\mathbf{B}$ at the same toroidal angle (ϕ) during the two current pulses. During the first pulse [Figs. 4(a) and 4(b)], the magnetic topology exhibits chaotic scattering, as found in the earlier simulation study of spheromak sustainment [8]. The sparsity of punctures indicates that the traced field lines complete only a small number of toroidal transits before encountering an electrode surface. The computed maximum of 35 eV is consistent with an analytical prediction for temperature on open magnetic field lines subject to Ohmic heating and parallel thermal conduction at a fixed current density [13,14]. With 8 MA/m^2 of current density taken from the geometric axis and a parallel connection-length estimate of 3 m, the analytical relation Eq. (19) from Ref. [14] predicts a maximum of 30 eV.

When the primary drive is removed, the edge and geometrically central regions cool rapidly via parallel conduction, making them very resistive. This enhances magnetic reconnection and diffusion, and it helps remove the current-gradient drive of the $n = 1$ mode. The length of field lines passing through the toroidal region of amplified poloidal flux then increases, leading to the increasing

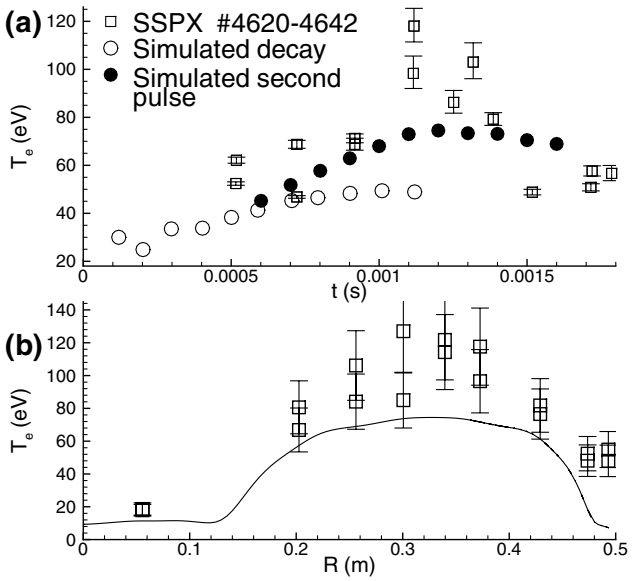

FIG. 3. Comparisons of electron temperature measured with Thomson scattering in SSPX discharges Nos. 4620–4642 with simulation results on $\langle T \rangle$: (a) temperature evolution central to the amplified poloidal flux and (b) midplane temperature profiles from experiment at $t = 1.1$ ms (boxes) and from the two-pulse simulation at $t = 1.2$ ms (solid trace).

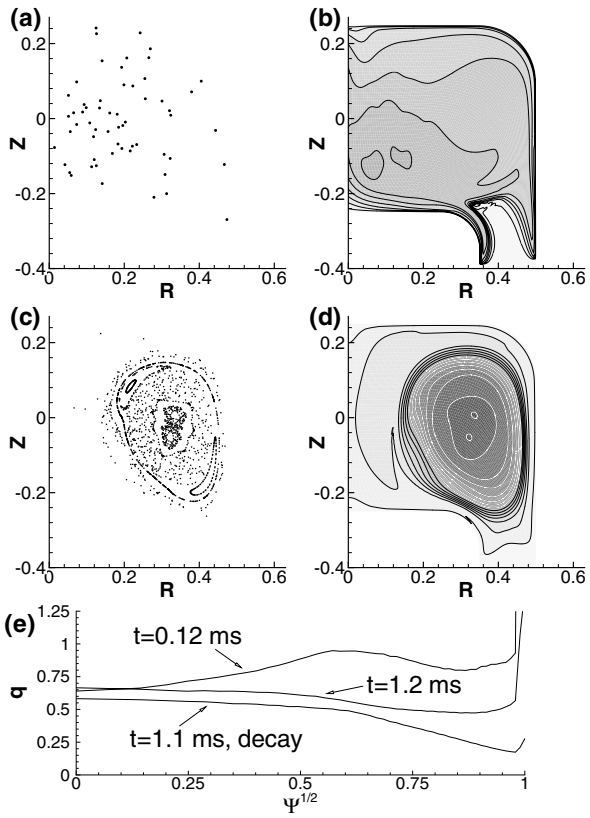

FIG. 4. Magnetic puncture plots and contours of constant temperature at the end of the first current pulse and during the second current pulse. The frames show (a) magnetic punctures at $t = 1.2$ ms, (b) temperature at $t = 1.2$ ms, (c) magnetic punctures at $t = 1.2$ ms, and (d) temperature at $t = 1.2$ ms. Shading is for the range of 0 to 75 eV, and contours for $T \geq 40$ eV are indicated by white lines. Frame (e) shows the safety factor vs the square root of poloidal flux in the region of amplified flux.

temperatures shown in Fig. 3(a). The second current pulse at $t = 0.5$ ms and the resulting quiescent period produce large closed-flux surfaces at $t = 1.2$ ms, as evident in Fig. 4(c). Ohmic heating continues, due to gradual resistive decay, but energy loss involves slower cross-field transport. This results in a large temperature gradient at the edge of the magnetically closed region [Fig. 4(d)] and the largest temperature over the entire simulation (Fig. 3). The late-time Poincaré plot also shows an $m = 2$, $n = 4$ island structure near the edge of the closed-flux region and an $m = 2$, $n = 3$ structure near the magnetic axis.

Magnetic fluctuations with $n > 1$ have a strong influence on the evolution of temperature, but the second current pulse provides a means of transiently controlling the $n = 2$ component. The beneficial effect can be understood from the safety factor (q) profiles shown in Fig. 4(e), with $q = d\langle\Phi\rangle/d\langle\Psi\rangle$, where $\langle\Phi\rangle$ and $\langle\Psi\rangle$ are toroidal and poloidal magnetic-flux functions of $\langle\mathbf{B}\rangle$, respectively. The q computation is not a true magnetic winding number at $t = 0.12$ ms when the field is open and chaotic, but it indicates that the toroidal flux is greatest during the initial pulse. When the injector-current decreases, the q values fall, particularly near the edge of the amplified flux. Without a second current pulse ["decay" trace in Fig. 4(e)], the outer q values are well below 0.5, and the $m = 1$, $n = 2$ mode is resonant near the middle of the amplified flux region. Application of the second current pulse retains more toroidal flux, so the $m = 1$, $n = 2$ mode is not resonant until later in time and then only near the edge of the amplified flux region. A nontrivial fraction of the amplified flux remains open. Thus, the $m = 2$, $n = 4$ island structure lies along the inner of the two $q = 0.5$ surfaces, and the large closed-flux surfaces, which form a transport barrier, are at or near the minimum of the q profile.

The MHD-collisional heat-flux modeling of these SSPX discharges compares fairly well over most of the discharge with quantitative results on driven plasma current, stored magnetic energy, local magnetic fluctuation levels, and temperatures. The largest discrepancy is in the evolution of temperature when it climbs rapidly in the experiment during the magnetically quiescent period. The slower response in the simulation may be due to the limitations of the single-temperature collisional heat-flux model or simplifications of the injector waveform. Nonetheless, the 3D simulations reproduce nearly all of the important characteristics of the experiment without fitting parameters. The results of this numerical study call attention to the importance of transient effects in SSPX discharges, despite the use of electrostatic current-drive. While the second current pulse does not sustain the discharge, it tailors the q profile with respect to avoiding harmful MHD activity that is resonant in the decaying poloidal flux. The correlation of performance-limiting $n > 1$ modes with the appearance of corresponding q values in fitted MHD equilibria has also been noted recently [12,22] for the experiment. The extent to which external controls, such as the second injector-current pulse, can benefit cyclical operation remains to be determined. Already, temperatures exceeding 200 eV have been obtained in SSPX [12], and simulations of the newer current-drive strategies are under way [23].

The authors acknowledge Simon Woodruff and Ken Fowler for many productive discussions. Some of the reported simulations have been performed at the National Energy Research Scientific Computing Center. This research is supported by the U.S. Department of Energy through Grant No. DE-FG02-02ER54687 and through University of California LLNL under Contract No. W7405-ENG-48.

[1] L. Lindberg and C. T. Jacobsen, Phys. Fluids **7**, S44 (1964).
[2] W. C. Turner *et al.*, Phys. Fluids **26**, 1965 (1983).
[3] T. R. Jarboe *et al.*, Phys. Rev. Lett. **51**, 39 (1983).
[4] T. G. Cowling, Mon. Not. R. Astron. Soc. **94**, 39 (1934).
[5] A. H. Boozer, Phys. Fluids B **5**, 2271 (1993).
[6] A. al-Karkhy *et al.*, Phys. Rev. Lett. **70**, 1814 (1993).
[7] C. R. Sovinec, J. M. Finn, and D. del-Castillo-Negrete, Phys. Plasmas **8**, 475 (2001).
[8] J. M. Finn, C. R. Sovinec, and D. del-Castillo-Negrete, Phys. Rev. Lett. **85**, 4538 (2000).
[9] T. R. Jarboe *et al.*, Phys. Fluids B **2**, 1342 (1990).
[10] E. B. Hooper, L. D. Pearlstein, and R. H. Bulmer, Nucl. Fusion **39**, 863 (1999).
[11] H. S. McLean *et al.*, Phys. Rev. Lett. **88**, 125004 (2002).
[12] H. S. McLean *et al.*, in *Proceedings of the 30th EPS Conference on Controlled Fusion and Plasma Physics, St. Petersburg, Russia, 2003*, Europhysics Conference Abstracts Vol. 27A (European Physical Society, Mulhouse, France, 2003), p. 3.230.
[13] G. Miller, Plasma Phys. Controlled Fusion **26**, 1119 (1984).
[14] E. B. Hooper, R. H. Cohen, and D. D. Ryutov, J. Nucl. Mater. **278**, 104 (2000).
[15] R. W. Moses, R. A. Gerwin, and K. F. Schoenberg, Phys. Plasmas **8**, 4839 (2001).
[16] C. R. Sovinec *et al.*, J. Comput. Phys. **195**, 355 (2004).
[17] S. I. Braginskii, *Reviews of Plasma Physics*, edited by M. A. Leontovich (Consultants Bureau, New York, 1965), Vol. 1, p. 205.
[18] G. W. Hammett and F. W. Perkins, Phys. Rev. Lett. **64**, 3019 (1990).
[19] E. D. Held *et al.*, Phys. Plasmas **8**, 1171 (2001).
[20] S. C. Hsu and P. M Bellan, Phys. Rev. Lett. **90**, 215002 (2003).
[21] B. W. Stallard *et al.*, Phys. Plasmas **10**, 2912 (2003).
[22] S. Woodruff *et al.*, Bull. Am. Phys. Soc. **48**, 150 (2003).
[23] B. I. Cohen *et al.*, "Spheromak Evolution and Energy Confinement" (to be published).